Ab initio ballistic conductance with spin-orbit coupling: Application to monoatomic wires

Andrea Dal Corso,[1,2] Alexander Smogunov,[1,2,3] and Erio Tosatti[1,2,4]
[1]*SISSA, Via Beirut 2/4, 34014 Trieste, Italy*
[2]*DEMOCRITOS-INFM, Via Beirut 2/4, 34014 Trieste, Italy*
[3]*Voronezh State University, University Square 1, 394006 Voronezh, Russia*
[4]*ICTP, Strada Costiera 11, 34014 Trieste, Italy*
(Received 18 April 2006; revised manuscript received 15 June 2006; published 28 July 2006)

The approach proposed by Choi and Ihm [Phys. Rev. B **59**, 2267 (1999)] for calculating the ballistic conductance of open quantum systems within the Landauer-Büttiker approach is generalized to fully relativistic ultrasoft pseudopotentials, enabling it to deal with ballistic transport in the presence of spin-orbit coupling. As a test case, we present the complex k-vector electronic structure of a perfect monoatomic nonmagnetic Pt wire, and the ballistic conductance of a toy nanocontact model consisting of the same Pt nanowire with one stretched bond. By comparing the fully relativistic and the scalar relativistic results, it is seen that the relative importance of spin-orbit effects can be quite large.

DOI: 10.1103/PhysRevB.74.045429 PACS number(s): 71.15.Mb, 63.20.Dj

I. INTRODUCTION

Nanocontacts as thin as a monoatomic can be fabricated by means of scanning tunneling microscopes or mechanically controllable break junctions.[1] The size of these contacts is generally much smaller than the electron mean free path so that they behave as ballistic conductors. By measuring the conductance while pulling the contact, one observes constant plateaus alternated to sudden jumps, the latter generally connected with atomic rearrangements. In some elements, such as Ir, Pt, and Au, the last plateau before breaking of the nanocontact is particularly long and suggests the existence of monoatomic wires that are several atoms long.[2,3] Monoatomic Au wires,[4,5] as well as three-atom long monoatomic wires of Co, Pd, and Pt (Ref. 6) have indeed been imaged by transmission electron microscopy.

At the theoretical level, the transport properties of atomic scale conductors can be calculated by the Landauer-Büttiker approach,[7] by considering the transmission and reflection of the electronic wave functions at the nanocontact.[8–13] In realistic approaches, the electronic structure is calculated within density functional theory (DFT), in the local density or in the local spin density approximation (LSDA) to account for spin magnetism.[10,14,15] Many-body effects have also been accounted for in the theory,[16] while ballistic conductance in the presence of spin-orbit (SO) coupling has been addressed only very recently.[17] It is well known that in heavy elements, SO changes significantly the electron band structures with respect to scalar relativistic (SR) theories. Therefore its inclusion is expected to be important for ballistic conductance. In principle, the SO-induced electronic structure modifications could even change the number of channels available for transmission at the Fermi level. Besides, they could also affect the predicted magnetic properties.[18] For instance, a Pt monoatomic wire was found theoretically to be ferromagnetic at interatomic distances larger than 2.2 Å including SO, while without SO it is nonmagnetic until much larger distances.[18] Moreover, theoretical speculations have pointed out that, in monoatomic wires, interesting phenomena due to SO coupling such as anisotropic ballistic magnetoresistance[19] or giant magnetocrystalline anisotropy[20] could be observable. Deferring discussion of the magnetic case to a later work, we intend to focus here on the nonmagnetic system, concentrating on the issue of transport in the presence of SO.

SO coupling is naturally dealt with when the electronic structure is calculated by solving a Dirac-like equation for four-component spinors such as the one obtained in the framework of relativistic DFT.[17,21,22] However, it is well known that SO effects can be studied also within a simplified framework provided by a DFT formulation based on the spin-density matrix with orbitals described by two-component spinor wave functions.[23–26] Actually, in a previous paper, one of us introduced fully relativistic (FR) ultrasoft pseudopotentials[27] (USPPs) acting on two-component spinors and showed that they provide SO split-band structures of bulk fcc-Au and fcc-Pt in good agreement with those found by solving the Dirac equation for four-component spinor wave functions.[28]

Choi and Ihm[9] originally introduced a complex k-vector method for calculating the transmission coefficient of an open quantum system where nuclei and core electrons are described by fully nonlocal norm conserving PPs of the Kleinman-Bylander type.[29] The transmission coefficient at fixed energy E is obtained from the scattering states of the open system. Key quantities of the method are the Bloch functions at complex wave vectors necessary to expand the scattering states in the leads. In earlier work (Ref. 10), we generalized this method to magnetic materials (within the LSDA) and to USPPs. Here we further extend this approach to deal with systems described by two-component spinor wave functions and FR USPPs, which include SO. Moreover, the method is demonstrated by an explicit calculation on a simple test case. In particular, we present the complex k-vector bands for an infinite Pt monoatomic wire, followed by the ballistic conductance of an idealized toy nanocontact consisting of the same Pt nanowire with one stretched bond.

II. METHOD

In spin DFT, the basic variable is the spin density of the interacting electron gas.[23] As in the spin-restricted theory,[30]

one can introduce auxiliary one-electron Kohn and Sham orbitals which are two-component spinors $\Psi^{\sigma}(\mathbf{r})$, where σ is a spin index. As shown in Ref. 28, a FR nonlocal USPP acting on spinor wave functions can be rewritten as a 2×2 matrix where each element has the form of a SR USPP with spin-dependent coefficients. The total energy contains local and nonlocal PP terms and the scattering equation is given by (in atomic units)[28]

$$E\Psi^{\sigma}(\mathbf{r}) = -\frac{1}{2}\nabla^2\Psi^{\sigma}(\mathbf{r}) + \sum_{\sigma'} V_{LOC}^{\sigma,\sigma'}(\mathbf{r})\Psi^{\sigma'}(\mathbf{r}) + \sum_{I\alpha\beta}\sum_{\sigma'} \bar{D}_{\alpha\beta}^{I,\sigma,\sigma'}\langle\beta_{\beta}^{I}|\Psi^{\sigma'}\rangle\beta_{\alpha}^{I}(\mathbf{r}-\mathbf{R}_I). \quad (1)$$

The local potential is a 2×2 matrix: $V_{LOC}^{\sigma,\sigma'}(\mathbf{r}) = V_{\mathrm{eff}}(\mathbf{r})\delta_{\sigma,\sigma'} - \mu_B\mathbf{B}_{xc}\cdot\boldsymbol{\sigma}_{\sigma,\sigma'}$, defined in terms of the effective potential $V_{\mathrm{eff}}(\mathbf{r})$ and of the exchange and correlation magnetic field $\mathbf{B}_{xc}$ (see Ref. 28 and Ref. 31). $\boldsymbol{\sigma}$ are the Pauli matrices, $\beta_{\alpha}^{I}(\mathbf{r}-\mathbf{R}_I)$ are projector functions centered on the atom $\mathbf{R}_I$, and the indexes α and β are a shorthand notation for composite indexes (indicated with τ,l,j,m in Ref. 28). Here, $\bar{D}_{\alpha\beta}^{I,\sigma,\sigma'}$ are defined in terms of the screened coefficients of the nonlocal PP and the spin-dependent coefficients of the overlap matrix: $\bar{D}_{\alpha\beta}^{I,\sigma,\sigma'} = \tilde{D}_{\alpha\beta}^{I,\sigma,\sigma'} - Eq_{\alpha\beta}^{I,\sigma,\sigma'}$ (see Ref. 28 for the definition of $\tilde{D}_{\alpha\beta}^{I,\sigma,\sigma'}$ and of $q_{\alpha\beta}^{I,\sigma,\sigma'}$).

We study the electron transmission in an open quantum system consisting of a scattering region $0<z<L$ and left ($z<0$) and right ($z>L$) leads. In the (x,y) directions, a supercell geometry with periodic boundary conditions is adopted. The periodicity in the (x,y) plane allows us to use Bloch's theorem introducing $\mathbf{k}_{\perp}$ points in the two-dimensional Brillouin zone and solving Eq. (1) separately at each $\mathbf{k}_{\perp}$ (see also Ref. 32). Equation (1) is solved by generalizing the techniques of Refs. 9 and 10, using a well known method applicable to this kind of integrodifferential equations.[9] It is useful to introduce the functions

$$P_{s\alpha}(\mathbf{r}) = \sum_{\mathbf{R}_{\perp}} e^{i\mathbf{k}_{\perp}\cdot\mathbf{R}_{\perp}}\beta_{\alpha}^{I}(\mathbf{r}-\mathbf{R}_I), \quad (2)$$

and the integrals

$$C_{s\alpha}^{\sigma} = \sum_{\beta,\sigma'} \bar{D}_{\alpha\beta}^{s,\sigma,\sigma'}\langle\beta_{\beta}^{s}|\Psi^{\sigma'}\rangle, \quad (3)$$

where $\mathbf{R}_I = \mathbf{R}_{\perp} + \boldsymbol{\tau}_s$ and s runs on the atoms of one unit cell, and to solve the homogeneous equations

$$E\Psi_n^{\sigma}(\mathbf{r}) = -\frac{1}{2}\nabla^2\Psi_n^{\sigma}(\mathbf{r}) + \sum_{\sigma'} V_{LOC}^{\sigma,\sigma'}(\mathbf{r})\Psi_n^{\sigma'}(\mathbf{r}), \quad (4)$$

where n runs over the independent solutions of this system. Their number is twice as large as in Refs. 9 and 10, since the equations for the two spin components are now coupled. Next we solve the inhomogeneous equations obtained by adding to Eq. (4) one inhomogeneous term, either in the equation for the first or in the equation for the second component of the spinor,

$$E\Psi_{s\alpha\zeta}^{\sigma}(\mathbf{r}) = -\frac{1}{2}\nabla^2\Psi_{s\alpha\zeta}^{\sigma}(\mathbf{r}) + \sum_{\sigma'} V_{LOC}^{\sigma,\sigma'}(\mathbf{r})\Psi_{s\alpha\zeta}^{\sigma'}(\mathbf{r}) + \delta_{\sigma,\zeta}P_{s\alpha}(\mathbf{r}), \quad (5)$$

where ζ is a spin index which indicates the equation where the inhomogeneous term has been added, and $\delta_{\sigma,\zeta}$ is the Kroneker symbol. The solution of Eq. (1) can be written as a linear combination of the solutions of Eqs. (4) and (5),

$$\Psi^{\sigma}(\mathbf{r}) = \sum_n a_n\Psi_n^{\sigma}(\mathbf{r}) + \sum_{s\alpha\zeta} C_{s\alpha}^{\zeta}\Psi_{s\alpha\zeta}^{\sigma}(\mathbf{r}). \quad (6)$$

The coefficients a_n for the left and right leads are calculated from the Bloch conditions, while the coefficients a_n for the scattering region are calculated from the wave function matching boundary conditions at $z=0$ and $z=L$. The coefficients $C_{s\alpha}^{\zeta}$ are determined together with the a_n as in Refs. 9 and 10.

In the leads, electron wave functions are Bloch functions also along the z direction and are characterized by a wave number k_z. The presence of the scattering region breaks the periodicity of the leads and generally states with complex k_z are required in order to expand accurately the scattering states in the lead region. Bloch states with both real and complex k_z values allowed at each fixed energy E are found by solving a generalized eigenvalue problem

$$AX = e^{ik_z d}BX, \quad (7)$$

as in Refs. 9 and 10. The components of the eigenvectors $X=(a_{n,k_z}, C_{s\alpha,k_z}^{\zeta})$ are the undetermined coefficients of the Bloch function.

Each Bloch state $\Psi_j^{\sigma}(\mathbf{r})$ characterized by a real wave vector k_z and propagating rightward in the left lead gives rise to a scattering state with the following asymptotic form in the left and right leads:

$$\Psi^{\sigma}(\mathbf{r}) = \begin{cases} \Psi_j^{\sigma}(\mathbf{r}) + \sum_{i\in L} r_{ij}\Psi_i^{\sigma}(\mathbf{r}), & z<0 \\ \sum_{i\in R} t_{ij}\Psi_i^{\sigma}(\mathbf{r}), & z>L, \end{cases} \quad (8)$$

where $i\in L$ ($i\in R$) means that the sum over i is over all values of k_z (real or complex), which correspond either to Bloch states propagating leftward (rightward) or decaying in the left (right) lead. In the scattering region ($0<z<L$) the scattering state is expanded as in Eq. (6). The unknown coefficients $(r_{ij}, t_{ij}, a_n, C_{s\alpha}^{\zeta})$ of the scattering state are determined by solving a linear system as in Refs. 9 and 10. By using the t_{ij} calculated for Bloch states i and j propagating rightward in the right and left tips, we can calculate the total transmission. In the linear response regime (valid at small applied voltages), the ballistic conductance is obtained from the multichannel generalization of the Landauer-Büttiker formula[7]

$$G = \frac{e^2}{h}\sum_{ij}\frac{I_i}{I_j}|t_{ij}|^2, \quad (9)$$

where I_i and I_j are the probability currents of states i and j. Within the LSDA approximation, t_{ij} is zero if the spins of the

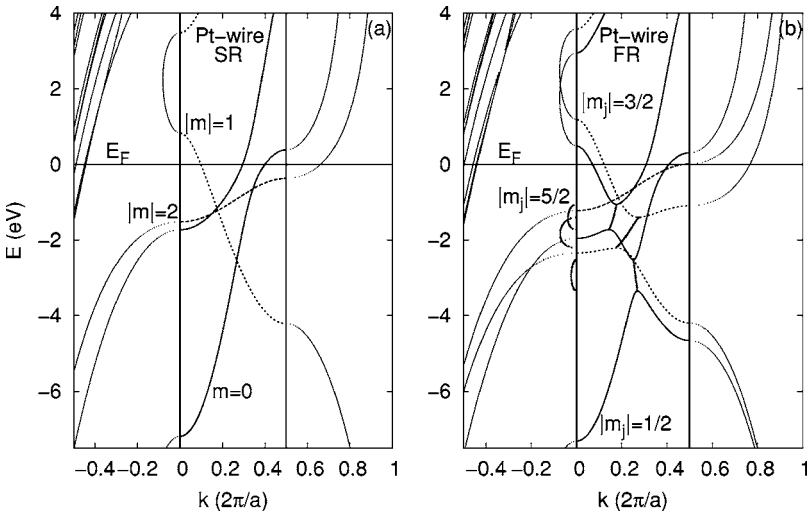

FIG. 1. Complex band structures of a nonmagnetic monoatomic Pt wire at the equilibrium Pt-Pt distance 2.35 Å. (a) SR and (b) FR bands are compared. Continuous lines, short-dashed, and dashed lines indicate FR (SR) bands with $|m_j|=1/2$, $|m_j|=3/2$, and $|m_j|=5/2$ ($m=0$, $|m|=1$, and $|m|=2$), respectively.

electrons in states i and j have opposite directions, hence no spin flip is allowed. In the present scheme instead, an electron in a Bloch state Ψ_j^σ contributes to the magnetization density a term $\mathbf{m}_j(\mathbf{r})=\mu_B\Sigma_{\sigma,\sigma'}\Psi_j^\sigma(\mathbf{r})\boldsymbol{\sigma}_{\sigma,\sigma'}\Psi_j^{\sigma'}(\mathbf{r})$ and the direction of $\mathbf{m}_j(\mathbf{r})$ depends on the position $\mathbf{r}$. A state j can be partially transmitted into a state i ($t_{ij}\neq 0$) with a magnetization density $\mathbf{m}_i(\mathbf{r})$ different from $\mathbf{m}_j(\mathbf{r})$. In order to calculate the ballistic conductance, we need the current carried along z, I_{k_z} by each Bloch state propagating in the left or right tips. The current I_j of a nondegenerate Bloch state j depends on its normalization. For a Bloch state normalized to one inside a unit cell, the current is proportional to the derivative of the eigenvalue E_{k_z} with respect to k_z,

$$I_{k_z}=\frac{1}{d}\frac{\partial E_{k_z}}{\partial k_z}, \tag{10}$$

where d is the size of the unit cell in the z direction. However, the solutions of Eq. (1) found by diagonalizing the generalized eigenvalue problem [Eq. (7)] are not normalized. Hence it is necessary to calculate their current independently of Eq. (10). Our scattering equation is formally similar to the scattering equation solved in Ref. 10, hence we can write the current in the same form. A sum over the two spinor components will give the total current through a plane S perpendicular to the z axis and located at z_0,

$$I_{k_z}=\mathrm{Im}\sum_\sigma\left[\int_S d^2\mathbf{r}_\perp\Psi_{k_z}^{\sigma*}\frac{\partial}{\partial z}\Psi_{k_z}^\sigma+2\sum_{I\alpha}C_{s\alpha,k_z}^{*\sigma}\right.$$
$$\left.\times\int_{-\infty}^{z_0}dz'\int_S d^2\mathbf{r}'_\perp e^{-i\mathbf{k}_\perp\mathbf{R}_\perp}\beta_{s\alpha}(\mathbf{r}'-\mathbf{R}_I)^*\Psi_{k_z}^\sigma(\mathbf{r}')\right], \tag{11}$$

where S is the area of the periodic supercell in the (x,y) plane. Finally, as in Ref. 10, when degenerate Bloch states have nonzero off-diagonal currents, we will choose linear combinations of Bloch states which diagonalize the current.

III. A SIMPLE TEST APPLICATION

As a simple illustrative application of the theory just outlined, we study an infinite Pt monoatomic wire, first perfect and then with a single stretched bond. The LSDA exchange-correlation energy functional[33] is used in all calculations. The nuclei are described either by SR or by FR USPPs with parameters given in Ref. 28. A kinetic energy cutoff of 29 Ry is used for the plane-wave expansion of the pseudo-wavefunctions (270 Ry for the charge density). For the perfect wire the integration over the Brillouin zone is done with a $1\times1\times200$ uniform mesh of $\mathbf{k}$ points and a smearing[34] parameter of 5 mRy. The wire with one stretched bond is simulated with a supercell containing ten atoms. In this case, $1\times1\times21$ points are used. For the infinite Pt wire, we find an equilibrium interatomic distance of $a=2.35$ Å with either SR or with FR PPs. Within LSDA, at this short interatomic distance, the Pt nanowire is nonmagnetic within SR, and weakly magnetic within FR, with a small moment of order $0.1\mu_B$ per atom. Although we generally expect magnetism to play a role for the conductance of Pt contacts and wires,[18] in this test check we shall restrict to a nonmagnetic wire. In Figs. 1(a) and 1(b) we compare the SR and FR complex band structures of the perfect wire. Each figure is divided into three panels which, from left to right, contain the bands at imaginary k_z, at real k_z, and at $k_z=\frac{\pi}{a}+i\kappa$. Typical differences between the real k-vector bands calculated with a three-dimensional (3D) plane wave code[35] or by solving the generalized eigenvalue problem in Eq. (7) are of the order of a meV, or less. The real bands agree very well with the results presented in Ref. 18, the small differences being due to the different exchange and correlation functionals used in the two calculations. The SR wave functions are eigenfunctions of the z component (along the wire axis) of the orbital angular momentum L_z and can be labeled by the integer eigenvalues m of this operator. Equivalently, at arbitrary k_z, they form a basis for the irreducible representations of the $C_{\infty v}$ group: Σ^+, Π, Δ, etc.[36] The wave functions with $m=0$ transform as the Σ^+ representation, those with $|m|=1$ and $|m|=2$ transform as Π and Δ, respectively. The occupied real bands

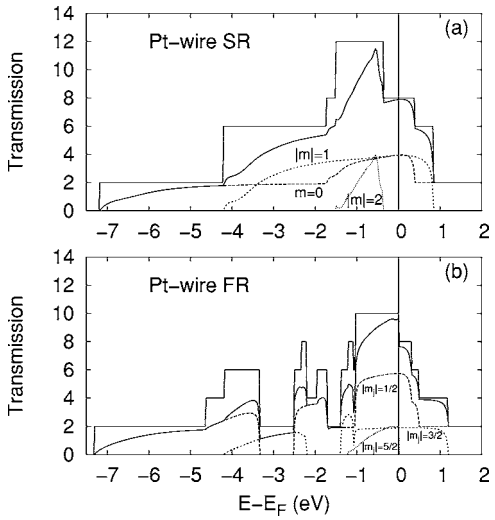

FIG. 2. Transmission as a function of energy of a Pt wire at the equilibrium Pt-Pt distance (2.35 Å) with one bond stretched to 2.55 Å. (a) SR and (b) FR transmissions are compared. The zero of the energy is at the Fermi level. Continuous lines give the total number of channels and the total transmission. Dashed, short-dashed, and dotted lines denote the FR (SR) $|m_j|=1/2$, $|m_j|=3/2$, and $|m_j|=5/2$ ($m=0$, $|m|=1$, and $|m|=2$) contributions, respectively.

merge, at $k_z=0$ and at $k_z=\pi/a$, with paraboliclike bands while a loop, at imaginary k_z, joins the $|m|=1$ bands at 0.8 and 3.5 eV. In addition to the degeneracy due to the spatial symmetry, all SR bands are also spin degenerate, for zero magnetization. Things change in the FR calculation. The SO split wave functions [Fig. 1(b)] are eigenfunctions of the z component of the total angular momentum J_z and can be labeled with its semi-integer eigenvalues m_j. Equivalently, they form a basis for the two-dimensional irreducible representations of the $C_{\infty v}$ double group: $\Gamma^{1/2}$, $\Gamma^{3/2}$, $\Gamma^{5/2}$, etc., where states $|m_j|=1/2$ transform as $\Gamma^{1/2}$, states $|m_j|=3/2$ transform as $\Gamma^{3/2}$, and so on.[37] In the presence of SO, former $m=0$ states give rise to $|m_j|=1/2$, former $|m|=1$ states split into $|m_j|=1/2$ and $|m_j|=3/2$ states, $|m|=2$ states split into $|m_j|=3/2$ and $|m_j|=5/2$ states. The Pt nanowire has three distinct bands derived from $|m_j|=1/2$ states. They anticross near $k_z=0.15$ and 0.25 (in units of $2\pi/a$). States with $|m_j|=3/2$ form two bands which anticross at the center of the zone. Finally, states with $|m_j|=5/2$ form an isolated, very narrow band, very similar to the original SR $|m|=2$ band. The FR valence bands merge at $k_z=0$ and at $k_z=\frac{\pi}{a}$ with paraboliclike bands as in the SR case. In addition, new bands that connect the gap formed by the two $|m_j|=3/2$ bands and the two gaps formed by the three $|m_j|=1/2$ bands appear in the complex k plane. These are indicated with thick lines in Fig. 1(b) where the real (imaginary) part of k_z is projected in the central (left) panel. The perfect wire, where electrons are free of scattering, has a trivial conductance equal to the number of bands crossing the Fermi level: $G=10G_0$ ($G=8G_0$) $\left(G_0=\frac{e^2}{h}\right)$ according to the FR (SR) calculation. The difference between FR and SR results is due to the $|m_j|=5/2$ band which touches the Fermi level at the zone border, whereas the SR $|m|=2$ band did not. In this tipless geometry, the values of the conductance are much larger than the values measured in present experiments in Pt nanocontacts, whose physics we do not directly address at this stage, and which show preferentially ballistic conductance values around $4G_0$.[1] A reduction of conductance below the ideal channel number is expected to arise as soon as any source of electron scattering is introduced. In Fig. 2(b) [Fig. 2(a)], we show the FR (SR) transmission function as a function of energy calculated for the same monoatomic Pt nanowire where all bonds are at the equilibrium distance, except one which is stretched to 2.55 Å. Due to this perturbation, the Bloch states of the perfect wire are now partly reflected and partly transmitted. The conductances at E_F are $7.7G_0$ and $9.6G_0$ in the SR and in the FR case, respectively. At energies away from E_F, the FR and SR transmissions often differ much more significantly. This reflects the different number of channels available at each energy due to the splitting and anticrossing of the bands allowed by the double group symmetry. We can operate an instructive decomposition of transmission along symmetry channels. In the stretched bond model, the scattering region retains full rotational symmetry about the wire axis so that the transmission coefficient t_{ij} between states which belong to different representations of the symmetry group is zero and the transmission eigenchannels have well-defined symmetry. For illustration, in Fig. 2, we decompose the total transmission into contributions of different transmission eigenchannels adding those with the same orbital (SR) or total (FR) angular momentum along z. The main contribution to conductance at E_F is the $|m_j|=1/2$ channel, followed by $|m_j|=3/2$ and by $|m_j|=5/2$. The latter arises only thanks to SO, since in its absence the $|m|=2$ derived band would not cross the Fermi level at all.

IV. CONCLUSION

We have extended the complex k-vector band structure method for calculating the ballistic conductance of nanocontacts to include FR USPPs, which account for SO coupling. Our approach is based on the noncollinear version of the spin DFT and allows us to treat the scattering of spinor wave functions. A test toy application is carried out on a monoatomic Pt nanowire with one stretched bond. Inclusion of SO proves to be qualitatively and quantitatively very important. At the qualitative level, electronic states inclusive of SO display differences of dispersion that have very noticeable consequences near the Fermi level, where the number of conducting channels is generally influenced. As a result, the values of ballistic conductance are quantitatively affected. We are presently applying this method for realistic ballistic conductance calculations of heavy transition metal nanocontacts.

ACKNOWLEDGMENTS

This work was sponsored by MIUR PRIN/Cofin Contract No. 2004023199, MIUR FIRB Contract No. RBAU017S8R, and MIUR FIRB Contract No. RBAU01LX5H as well as by INFM/CNR "Iniziativa trasversale calcolo parallelo."

[1] N. Agrait, Phys. Rep. **377**, 81 (2003).
[2] A. I. Yanson, G. R. Bollinger, H. E. van den Brom, N. Agraït, and J. M. van Ruitenbeek, Nature (London) **395**, 783 (1998).
[3] R. H. M. Smit, C. Untiedt, A. I. Yanson, and J. M. van Ruitenbeek, Phys. Rev. Lett. **87**, 266102 (2001).
[4] H. Ohnishi, Y. Kondo, and K. Takayanagi, Nature (London) **395**, 780 (1998).
[5] T. Kizuka, Phys. Rev. Lett. **81**, 4448 (1998).
[6] V. Rodrigues, J. Bettini, P. C. Silva, and D. Ugarte, Phys. Rev. Lett. **91**, 096801 (2003).
[7] R. Landauer, Philos. Mag. **21**, 863 (1970).
[8] N. D. Lang, Phys. Rev. B **52**, 5335 (1995).
[9] H. J. Choi and J. Ihm, Phys. Rev. B **59**, 2267 (1999).
[10] A. Smogunov, A. Dal Corso, and E. Tosatti, Phys. Rev. B **70**, 045417 (2004).
[11] K. Hirose, H. Kitahara, and T. Hattori, Phys. Rev. B **67**, 195315 (2003).
[12] K. S. Thygesen, M. V. Bollinger, and K. W. Jacobsen, Phys. Rev. B **67**, 115404 (2003).
[13] M. Branbyge, J.-L. Mozos, P. Ordejón, J. Taylor, and K. Stokbro, Phys. Rev. B **65**, 165401 (2002).
[14] A. Bagrets, N. Papanikolaou, and I. Mertig, Phys. Rev. B **70**, 064410 (2004).
[15] D. Jacob, J. Fernandez-Rossier, and J. J. Palacios, Phys. Rev. B **71**, 220403 (2005).
[16] A. Ferretti, A. Calzolari, R. Di Felice, F. Manghi, M. J. Caldas, M. B. Nardelli, and E. Molinari, Phys. Rev. Lett. **94**, 116802 (2005).
[17] V. Popescu, H. Ebert, N. Papanikolaou, R. Zeller, and P. H. Dederichs, Phys. Rev. B **72**, 184427 (2005).
[18] A. Delin and E. Tosatti, Phys. Rev. B **68**, 144434 (2003); Surf. Sci. **566-568**, 262 (2004).
[19] J. Velev, R. F. Sabirianov, S. S. Jaswal, and E. Y. Tsymbal, Phys. Rev. Lett. **94**, 127203 (2005).
[20] Y. Mokrousov, G. Bihlmayer, S. Heinze, and S. Blügel, Phys. Rev. Lett. **96**, 147201 (2006).
[21] A. H. MacDonald and S. H. Vosko, J. Phys. C **12**, 2977 (1979); A. K. Rajagopal and J. Callaway, Phys. Rev. B **7**, 1912 (1973).
[22] J. Anton, B. Fricke, and E. Engel, Phys. Rev. A **69**, 012505 (2004).
[23] L. Hedin and B. I. Lundqvist, J. Phys. C **4**, 2064 (1971).
[24] D. Hobbs, G. Kresse, and J. Hafner, Phys. Rev. B **62**, 11556 (2000).
[25] T. Oda, A. Pasquarello, and R. Car, Phys. Rev. Lett. **80**, 3622 (1998).
[26] R. Gebauer and S. Baroni, Phys. Rev. B **61**, R6459 (2000).
[27] D. Vanderbilt, Phys. Rev. B **41**, 7892 (1990).
[28] A. Dal Corso and A. Mosca Conte, Phys. Rev. B **71**, 115106 (2005).
[29] L. Kleinman and D. M. Bylander, Phys. Rev. Lett. **48**, 1425 (1982).
[30] W. Kohn and L. J. Sham, Phys. Rev. **140**, A1133 (1965).
[31] A. Dal Corso, Phys. Rev. B **64**, 235118 (2001).
[32] A. Smogunov, A. Dal Corso, and E. Tosatti, Phys. Rev. B **73**, 075418 (2006).
[33] J. P. Perdew and A. Zunger, Phys. Rev. B **23**, 5048 (1981).
[34] M. Methfessel and A. T. Paxton, Phys. Rev. B **40**, 3616 (1989).
[35] S. Baroni, S. de Gironcoli, A. Dal Corso, and P. Giannozzi, http://www.pwscf.org
[36] M. Weissbluth, *Atoms and Molecules* (Academic Press, New York, 1978).
[37] J. Oreg and G. Malli, J. Chem. Phys. **61**, 4349 (1974).